Agricultural and Forest Meteorology 206 (2015) 33–44

Contents lists available at ScienceDirect

Agricultural and Forest Meteorology

journal homepage: www.elsevier.com/locate/agrformet

Detecting drift bias and exposure errors in solar and photosynthetically active radiation data

J.D. Wood [a,*], T.J. Griffis [a], J.M. Baker [a,b]

[a] Department of Soil, Water, and Climate, University of Minnesota, Saint Paul, MN, United States
[b] USDA-ARS Soil and Water Research Unit, Saint Paul, MN, United States

ARTICLE INFO

Article history:
Received 31 July 2014
Received in revised form 20 February 2015
Accepted 21 February 2015

Keywords:
Radiation exposure
Sensor fading
Drift detection
Change point

ABSTRACT

All-black thermopile pyranometers are commonly used to measure solar radiation. Ensuring that the sensors are stable and free of drift is critical to accurately measure small variations in global solar irradiance at the Earth's surface ($K\downarrow$), which is a potential driver of changes in surface temperature. We demonstrate that the decreased responsivities of Eppley PSP pyranometers of $-1.5\%\,y^{-1}$, or $-0.38\%\,(GJ\,m^{-2})^{-1}$, were accompanied by a change in its spectral response owing to a discoloration of the sensing element. These observations motivated further work to develop routines to detect probable pyranometer drift in historical time-series. The temporal trends in the following ratios were used to detect pyranometer sensor drift: photosynthetically active radiation (PAR) to $K\downarrow$, $K\downarrow$ to K_{EX} (extraterrestrial radiation at the top of the atmosphere) and PAR to K_{EX}. Data from 8 AmeriFlux sites spanning latitudes from ~32 to 54°N were examined in this analysis. Probable drift in either a pyranometer or PAR sensor was identified at 5 of the 8 sites. The magnitude of the drift represented changes of $0.15–0.85\%\,y^{-1}$, which is sufficient to obscure actual trends in $K\downarrow$, although these should be considered conservative low end drift estimates, given that we were not making comparisons to co-located higher grade instruments. Deployment exposure errors caused by sensor shading were also discovered by comparing the daily correlations between (i) $K\downarrow$ and K_{EX} and (ii) PAR and K_{EX}. Sensors drifting at rates similar to our defective PSP over a 5 year period would contribute to an underestimation of available energy of $\sim 70\,W\,m^{-2}$, which is non-trivial in the context of assessing eddy covariance energy balance closure, employing Penman-Monteith or Bowen ratio methods or calculating albedo radiative forcings. Given that probable drift was identified at multiple AmeriFlux sites, we recommend enhancing network access to calibration services that are traceable to a high quality gold standard.

© 2015 Elsevier B.V. All rights reserved.

1. Introduction

Solar radiation, sometimes referred to as shortwave radiation, is the primary input of energy to the climate system. The surface shortwave radiative fluxes – incoming ($K\downarrow$) and outgoing ($K\uparrow$) – are important drivers of available energy (net radiation, R_n), and are of interest in the context of understanding variations in evapotranspiration (ET) and atmospheric circulation. Therefore, $K\downarrow$ is a key forcing variable in global climate and regional weather forecasting models, while R_n is used for assessing energy budget closure for eddy flux QA/QC (Leuning et al., 2012), and as an input for estimating ET by the Penman-Monteith or Bowen ratio methods. In addition, the shortwave spectrum contains the entire photosynthetically active radiation (PAR) band, which is a critical variable controlling gross primary production. Furthermore, there has been growing interest in evaluating the radiative forcings associated with land-use changes that modulate surface albedos and net ecosystem CO_2 exchange (NEE) (Arora and Montenegro, 2011; Betts, 2000; Georgescu et al., 2011). Accurate records of shortwave radiative fluxes at the surface are thus needed to support a wide range of research activities.

The most common sensor deployed to measure hemispherical, broadband solar radiative fluxes is the thermopile pyranometer (Stanhill and Cohen, 2001), which is currently available from a variety of manufacturers. The availability and relative simplicity of these sensors belies the fact that making accurate $K\downarrow$ and $K\uparrow$ solar radiation measurements is a non-trivial exercise. Beyond errors induced by improper deployment and maintenance (e.g.,

* Corresponding author. Tel.: +1 612 624 1645.
E-mail address: jdwood@umn.edu (J.D. Wood).

http://dx.doi.org/10.1016/j.agrformet.2015.02.015
0168-1923/© 2015 Elsevier B.V. All rights reserved.

leveling, dome cleaning or clearing and shading from other tower components), known issues with thermopile pyranometers include thermal offsets (Bush et al., 2000; Philipona, 2002) and directional response errors (Myers et al., 2002). Applying corrections (Dutton et al., 2001; Ji, 2007), custom sensor modifications (Bush et al., 2000; Haeffelin et al., 2001; Ji and Tsay, 2010; Ji et al., 2011), conditioning with heated ventilation (Philipona, 2002) or deploying more recently developed pyranometers can effectively control these errors. However, a significant challenge that remains is long-term sensor stability, something that can only be mitigated by regular and frequent calibrations.

The contamination of solar radiation time-series with calibration drift makes it impossible to accurately track long-term trends that have been estimated to be on the order of $-0.5\,W\,m^{-2}$ per year from the 1960s through the late 1980s (Stanhill and Cohen, 2001), with updated analyses suggesting brightening of a similar magnitude during the 1990s (Wild et al., 2005). Practices are thus needed to prevent sensor drift from contaminating long time-series of radiation data. For the highest measurement accuracy, manufacturers recommend 1–2 year intervals between calibrations, although high quality networks generally require calibration at least once per year if not more. Although calibrations correct responsivity drift, these procedures do not fully account for physical changes to the sensing element. Calibrations are typically performed by matching the response of a field deployed pyranometer to a reference sensor under controlled indoor or ambient outdoor conditions (ISO 9847:1992). Unfortunately, this procedure will be unable to adequately correct for drift that is due to changes in spectral response caused by physical changes to the sensing element, such as fading of the black paint (Riihimaki and Vignola, 2008).

Frequent sensor calibration remains the best practice to ensure that high quality data are collected, and is the standard operating procedure in radiation monitoring networks such as SURFRAD (Surface Radiation Network; (Augustine et al., 2005)) or BSRN (Baseline Surface Radiation Network; (Ohmura et al., 1998)). The challenge is that sites belonging to the highest quality radiation monitoring networks remain sparsely distributed in space. For example, there are currently seven sites distributed across the conterminous United States in the SURFRAD network (http://www.esrl.noaa.gov/gmd/grad/surfrad/sitepage.html) and 51 sites providing global coverage in BSRN (http://bsrn.awi.de/stations/maps.html). In order to improve spatial coverage for regional or ecosystem scale studies, researchers may therefore, be forced to use data from stations where the calibration history is either not known, or it is known that the calibration frequency is less than ideal.

Developing approaches that researchers can use to screen shortwave radiation data to detect probable calibration drift is thus warranted from the standpoint of increasing spatial data coverage while attempting to minimize sacrifices in accuracy. This tool would be of value from the perspective of maintaining sensors at active sites, as well as for post-hoc screening of long-term datasets when performing site syntheses. We hypothesize that drift and step changes in responsivity will be more easily detectable in time-series of the ratios of different radiative fluxes than in the raw time-series of the individual sensors.

Here, we highlight the decay in responsivities of all-black thermopile pyranometers from observations where we have co-located stable measurements. We show that this decay was accompanied by a change in the spectral response of the sensing element, and discuss implications for long-term monitoring campaigns. A method to detect calibration drift and step changes in $K\downarrow$ time-series based on examining the ratios of: (i) $K\downarrow$ to K_{EX}, (extraterrestrial radiation at the top of the atmosphere), (ii) photosynthetically active radiation (PAR) to $K\downarrow$, and (iii) PAR to K_{EX} will be presented and evaluated.

2. Materials and methods

2.1. Calibration drift due to radiation exposure

This analysis uses historical data collected at Rosemount MN, USA, as well as results from a sensor inter-comparison performed where four all-black thermopile pyranometers (model PSP, The Eppley Lab Inc., Newport RI) that were initially deployed in 2002 were evaluated. Two had been deployed facing upwards to measure $K\downarrow$ and the other two facing downwards to measure $K\uparrow$. Systematic differences of ~10% between the two upward facing PSPs had been observed in the past, which was unexpected because the sensors were deployed within 1 km of one another. Therefore, an inter-comparison was initiated to evaluate the performance of the PSPs. In autumn 2013, the four PSPs were co-located with one black and white (BW) pyranometer (model 8-48, The Eppley Lab Inc.) that had not been field-deployed and was thus presumed to be free of radiation exposure induced calibration drift.

The pyranometers were deployed from September 20 through September 30 on a flat surface at a height of 1.5 m. Measurements were taken every 30 s, and half-hourly averages recorded using a datalogger (model 21X, Campbell Scientific Inc., Logan, UT). In order to better understand the findings from the inter-comparison, historical data from 2006 to 2010 were revisited. In presenting and discussing the results, we differentiate between the PSPs based on their deployment history – G21 or I10 refers to the most recent fields in which sensors were located, while 'upwards' or 'downwards' describes the orientation of the pyranometers during historical deployment, and not the orientation during the inter-comparison, for which they were all facing up.

2.1.1. Data processing

To minimize the effects of cosine response errors, solar radiation data were discarded when the solar zenith angle was >70°. When checking the sensors one morning, we noticed that condensation had formed on the outer surface of the domes on all pyranometers. This problem can be minimized with heating or ventilation (Phillipona, 2002), which we routinely employ for upward-facing instruments. In this case, there were not enough ventilators for all instruments. Therefore, more stringent filtering was implemented, whereby all data with timestamps of 1100 h (LST) and earlier were discarded. Data obtained during rainfall events were also discarded to prevent artifacts associated with variable condensation on the domes from affecting the comparison. All regression analyses were performed using the robustfit.m algorithm in MATLAB (The Mathworks Inc., Natick, MA), using the default 'bisquares' weighting function. In most cases two linear models were considered, one forced through the origin while the other included an intercept term. From a sensor physics perspective, the model forced through the origin is more appropriate because the response of a pyranometer in the absence of incident radiation should be $0\,W\,m^{-2}$. Thermal offset errors are, however, known to affect PSPs (Bush et al., 2000; Philipona, 2002) which could result in a non-zero intercept. Therefore, considering a model that includes an intercept term is warranted to extract as much information as possible. Parameter estimates were compared using two-tailed t-tests.

2.2. Detecting drift in historical data

We developed an approach to identify drift by examining the temporal trends in the three ratios: (i) PAR/$K\downarrow$, (ii) $K\downarrow/K_{EX}$, and (iii) PAR/K_{EX}. We recognize that atmospheric optical depth can vary in response to anthropogenic and natural factors (Ramanathan and Feng, 2009), which makes detecting sensor drift a challenge. We therefore, took steps to minimize the effect that real trends in the observed radiation variables would have on sensor drift detection.

Using co-located measurements was desirable from the perspective of avoiding the possibility that there was sufficient spatial variation in atmospheric composition to obscure drift detection implemented by comparison with other sites. A brief discussion of the steps that were taken to minimize false drift identification will now be provided.

Normalizing by measured K_{EX} eliminates the possibility that variations in solar emittance are responsible for real trends in PAR and $K\downarrow$, confining the possible causes to changes in atmospheric transmissivity or drift. The remaining ratio, PAR/$K\downarrow$ provides further constraints, and has the advantage of having both measurements being made at the surface. We defined sets of temporal trends in each ratio, that if observed would indicate probable drift in one sensor (i.e., pyranometer or PAR sensor), and simultaneously eliminate, or at the very least, minimize the contaminating effects of changing atmospheric transmissivity. The sets of defined trends indicative of probable drift are outlined in Table 1. For example, the expected set of trends for a downward drifting pyranometer (and stable PAR sensor) is: upward trending PAR/$K\downarrow$, downward trending $K\downarrow/K_{EX}$, and stable PAR/K_{EX}.

For comparison purposes, the expected temporal trends in the ratios that would accompany real trends in the radiation fluxes due to varying atmospheric composition are also provided in Table 1. A key point is that in order to confidently identify drift, it was necessary to observe sets of trends consistent with those prescribed in Table 1 in the "Drift" section. It must be underscored that with this approach we can only identify drift if one of the two sensors is stable. That is, to ascribe pyranometer drift, a stable PAR/K_{EX} ratio is required. Conversely for a drifting PAR sensor, a stable $K\downarrow/K_{EX}$ ratio is needed. We will now consider the factors that influence the transmission of shortwave radiation through the atmosphere, whether they are important in the context of contaminating drift detection, and if so, how our approach minimizes these effects.

Changes in atmospheric composition sufficient to radically alter the magnitudes of Rayleigh scattering, and absorption by uniformly mixed gases and ozone; and thus, control multi-year trends in $K\downarrow$ are unlikely (Stanhill and Cohen, 2001). The most plausible drivers of $K\downarrow$ trends due to variations in atmospheric transmissivity are cloud scattering, water vapor absorption and aerosol scattering/absorption. Although, changes in aerosol optical depth (AOD) has been identified as the most probable cause of large-scale $K\downarrow$ trends over the land surface (Stanhill and Cohen, 2001; Wang et al., 2012 Wild et al., 2005), it is important to consider how these three factors – clouds, AOD, and water vapor absorption – could interfere with sensor drift detection.

The algorithms select a sample of data from the clearest days, using $K\downarrow/K_{EX}$ as the metric, to eliminate cloud effects, and prevent natural seasonal variations in the ratios from obscuring drift detection. Furthermore, this approach selects for the days that are least affected by aerosols and water vapor. Let us now consider some scenarios to explore the extent to which variations in atmospheric composition might interfere with drift detection, beginning with changes in AOD. It is improbable that changes in AOD will have no effect in the PAR waveband, therefore, both $K\downarrow/K_{EX}$, and PAR/K_{EX} should trend in the same direction, but with differing magnitudes depending on which waveband is more sensitive to the aerosols. Requiring that one of these two ratios be stable for positive drift detection (Table 1) therefore, mitigates contamination by AOD effects. Next we will consider water vapor absorption effects.

Water vapor does not absorb in the PAR waveband. Since only $K\downarrow$ is affected by water vapor absorption, it is possible that the PAR/$K\downarrow$ and $K\downarrow/K_{EX}$ ratios display temporal trends in opposite directions, while PAR/K_{EX} remains stable – a pattern consistent with what is expected for a drifting pyranometer (Table 1). It is therefore, important to consider the sensitivity of $K\downarrow$ to variations in water vapor, to assess the likelihood that this will interfere with drift detection. Stanhill and Cohen (2001) estimated that increases of 3 and 6 mm from a global water vapor column average of 25 mm would increase atmospheric shortwave absorption by ~1% based on the work of Ramanathan and Vogelmann (1997) and Arking (1996), respectively. Further, Stanhill and Cohen (2001) noted that observed increases in atmospheric water vapor were not sufficient to significantly alter shortwave absorption during the latter part of the 20th century. More recently, Wang et al. (2012) estimated that atmospheric water vapor absorption increased by 1 W m^{-2} over 30 years during the 20th century dimming period over land. Taken together, the fact that these are small trends with magnitudes on the order of 1 W m^{-2} makes it unlikely that changes in water vapor absorption will interfere with drift detection since we are selecting for the clearest days each year, and that if drift is present, it will display stronger trends over shorter time-scales. A further analysis of the sensitivity of atmospheric shortwave absorption to changes in water vapor based on a simple radiative transfer model is provided in the supplementary information.

2.2.1. Data requirements

In addition to $K\downarrow$, the approach requires co-located measurements of PAR, and an estimation of K_{EX}. PAR is typically measured as a photosynthetic photon flux density (PPFD; μmol m^{-2} s^{-1}), which was multiplied by 0.235 J μmol^{-1} to convert to a radiative flux density (Campbell and Norman, 1998) to give dimensionless radiative flux ratios. The K_{EX} is computed using the cosine law of illumination with PMOD (Physikalisch-Meteorologisches Observatorium Davos) total solar irradiance (TSI) estimates (http://www.pmodwrc.ch/pmod.php?topic=tsi/composite/SolarConstant) and the known zenith angle for the location's latitude, longitude and altitude. The PMOD TSI data are reported for 1 AU, and were therefore, converted to true Earth–Sun distance.

Table 1
Expected trends in the PAR/$K\downarrow$, $K\downarrow/K_{EX}$, and PAR/K_{EX} ratios required to identify sensor drift and the expected 'real' trends in the ratios (for properly functioning sensors) for various scenarios where changes in atmospheric composition affect its transmissivity.

	Scenario	Trend[a] $\frac{PAR}{K\downarrow}$	$\frac{K\downarrow}{K_{EX}}$	$\frac{PAR}{K_{EX}}$
Drift[b]	Pyranometer drift down, PAR sensor stable	↑	↓	0
	Pyranometer drift up, PAR sensor stable	↓	↑	0
	Pyranometer stable, PAR sensor drift down	↓	0	↓
	Pyranometer stable, PAR sensor drift up	↑	0	↑
Real trends in atmospheric composition affects PAR and $K\downarrow$	Increasing aerosols, lower PAR sensitivity ($\Delta PAR < \Delta K\downarrow$)[c]	↑	↓	↓
	Decreasing aerosols, lower PAR sensitivity ($\Delta PAR < \Delta K\downarrow$)	↓	↑	↑
	Increasing aerosols, higher PAR sensitivity ($\Delta PAR > \Delta K\downarrow$)	↓	↓	↓
	Decreasing aerosols, higher PAR sensitivity($\Delta PAR > \Delta K\downarrow$)	↑	↑	↑
	Increasing water vapor	↑	↓	0

[a] Increasing trend = ↑; decreasing trend = ↓; no trend = 0.
[b] Temporal trends in the ratios required to diagnose drift.
[c] ΔPAR and $\Delta K\downarrow$ refer to changes in PAR and $K\downarrow$ over time, respectively.

The PMOD data were used because the most reliable TSI product available from the SORCE (Solar Radiation and Climate Experiment) mission began in 2003 (Myhre et al., 2013), and did not permit the assessment of data collected in the 1990's.

2.2.2. Data screening and calculations

Prior to subjecting data to the detection algorithm, they must be screened to permit the detection of the small drift in the presence of natural fluctuations in radiative fluxes, and to prevent other errors from contaminating the analyses. First, all data with zenith angles >60° were discarded to avoid directional response errors. To minimize the impact of varying optical depth, calculations were performed using a subset of data associated with the highest, clear-sky $K\downarrow/K_{EX}$ ratios. We only considered years where instrument failure did not decrease data retention below 90%.

For each year of available data, the 24 highest $K\downarrow/K_{EX}$ ratios were obtained along with the corresponding PAR/$K\downarrow$ and PAR/K_{EX} ratios and timestamps. Data were sampled from the clearest-sky days (with at least 5 h of data), which were identified based on the correlation between the first derivatives of valid $K\downarrow$ and K_{EX} data. The PAR, $K\downarrow$ and K_{EX} flux densities were drawn from the 2 h bracketing the minimum daily zenith angle on the days with the highest correlation coefficients. Using a sample size of 24 was a balance between including enough data to minimize statistical noise within a year, but not including so much data that optical depth effects contaminate the analysis. These de-noised data series were then subjected to the drift detection algorithms (described below).

Drift detection was accomplished by subjecting each of the 3 ratios to linear regression and change point detection analyses in an iterative procedure. Change point detection was included in case the pyranometer experienced an initial stable period before drifting – example traces of the three ratios for cases of a systematically downward drifting pyranometer with no stable period and an initial stable period are provided in Fig. 1a and b, respectively. During each iteration, separate linear regression analyses were performed where each ratio was a response variable and time was the explanatory variable. Change point detection was carried out similar to Wang (2003), except that not all permutations of segmenting the data were considered in order to prevent real short-term variations from being flagged as a change point. The classic change point model is:

$$X(t) = \begin{cases} a_1 + b_1 t + \epsilon_t, & 1 \le t \le c \\ a_2 + b_2 t + \epsilon_t, & c < t \le n \end{cases} \quad (1)$$

where $X(t)$ is a time-series variable, a and b are regression parameters, ϵ_t are residuals, and c is the change point. An iterative procedure was used to find statistically significant change points. At each iteration an F-value is calculated to permit significance testing. We modified the procedure to prevent short-term variations from being positively identified as change-points, because we were interested in long-term trends. We shifted c by 12 positions – half of the observations for a year – on each iteration. More specific details pertaining to change point detection are provided in the supplementary information.

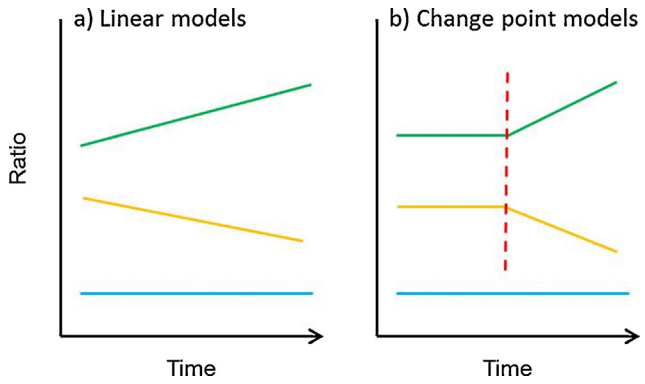

Fig. 1. Temporal trends in the PAR/$K\downarrow$ (green), $K\downarrow/K_{EX}$ (orange) and PAR/K_{EX} (blue) ratios for a pyranometer exhibiting steady downward calibration drift (a: linear models), and for a pyranometer that is stable for a time and then has a downward calibration drift (b: change point models). In panel (b) the vertical red dashed line denotes a change point in the PAR/$K\downarrow$ and $K\downarrow/K_{EX}$ signals. Note that these data are illustrative and not to scale. (For interpretation of the references to color in this figure legend, the reader is referred to the web version of this article).

The analysis was initialized using the first 3 years of data, after which subsequent data were added one year at a time, until either (a) iterations were terminated based on meeting specific criteria that are suggestive of drift, or (b) no drift was detected in the data. Selecting appropriate criteria for terminating the loop is essential to the successful implementation of diagnosing calibration drift. Because we were examining variables that exhibit natural variation, we required that a significant trend had to be observed for a minimum of 3 years before diagnosing drift. Furthermore, for a pyranometer drifting $-1.5\%\,y^{-1}$, it would take 3 years before the bias overwhelms the measurement uncertainty. This 3 year rule was applied to interpreting both the simple linear regression and change point models. In the change point case, we did not consider significant change points where the second segment of data was shorter than 3 years.

During each iteration the linear and change point models were fit to the PAR/$K\downarrow$ and $K\downarrow/K_{EX}$ time-series. Upon meeting the criteria for terminating iterations, the models were then fit to the associated PAR/K_{EX} data, in one step without iterating. This was done because analysis of PAR/K_{EX} was used as a check on the PAR sensor stability, and not as a primary identifier of pyranometer drift. Loop termination criteria and additional evidence considered when

Table 2
Summary of criteria that terminate the iterative drift detection procedure and additional considerations for interpreting the results.

Loop termination scenario	Criteria for loop termination	Additional considerations
(1) Consistent calibration drift	• 3 year data block analyzed • PAR/$K\downarrow$ and $K\downarrow/K_{EX}$ slopes significant • PAR/$K\downarrow$ and $K\downarrow/K_{EX}$ slopes have opposite direction (sign)	• PAR/K_{EX} slope is 0, and no significant change points with ≥3 years of data in segment 2
(2) Change point	• 3 years of data after the change point • Statistically significant change points in PAR/$K\downarrow$ and $K\downarrow/K_{EX}$ time-series • Segment 2 PAR/$K\downarrow$ and $K\downarrow/K_{EX}$ slopes significant and different sign	• PAR/K_{EX} slope is 0, and no significant change points with ≥3 years of data in segment 2 • PAR/$K\downarrow$ and $K\downarrow/K_{EX}$ change points within ±0.5 years • Within a time-series, segment 1 and 2 slopes significantly different • Significant linear PAR/$K\downarrow$ and $K\downarrow/K_{EX}$ of opposite sign that agree with change point segment 2 slopes[a]

[a] The point at which calibration was deemed necessary is based on the average change point, however, the presence of significant linear trends that agree with the direction of segment 2 change point slopes is further evidence of drift.

Table 3
Site-years of data used for evaluating drift detection algorithms.

Site (years)	Lat (°N), long (°W), alt (m)	Pyranometer model	Reference
CA-Oas (1997–2008)	53.6289, 106.1978, 600	PSP[a]	(Amiro et al., 2006)
CA-Obs (1997–2008)	53.9872, 105.1178, 598	PI preference	(Bergeron et al., 2007)
CA-Cbo (1996–2003)	44.3185, 79.9342, 211	PSP	(Gu et al., 1999)
US-Bo1 (1996–2008)	40.0062, 88.2904, 219	CM3[b]	(Meyers and Hollinger, 2004)
US-NR1(1996–2003)	40.0329, 105.5464, 3050	CM3	(Turnipseed et al., 2002)
US-Ro1 (2006–2010)	44.7143, 93.0898, 260	PSP (2)	(Baker and Griffis, 2005)
US-Srm (2004–2012)	31.8214, 110.8661, 1116	CM3	(Potts et al., 2008)
US-Wkg (2004–2012)	31.7365, 109.9419, 1531	CM3	(Scott, 2010)

[a] The stated non-stability of the PSP is $\pm 0.5\%\,y^{-1}$.[b]The CM3 pyranometer was a component of a model CNR1 4-component net radiometer (Kipp and Zonen USA Inc., Bohemia, NY). The CM3 has a stated non-stability of $\pm 1\%\,y^{-1}$.

interpreting the results are provided in Table 2. Model parameters were declared statistically significant at $p < 0.05$.

We applied the drift detection algorithms to data from eight AmeriFlux sites (Table 3). Recent interest in understanding ecosystem responses to climate change has led to the establishment of monitoring networks devoted to continuously measuring water and carbon fluxes (Baldocchi et al., 2001). At these sites, the emphasis is usually on measuring net ecosystem CO_2 exchange (NEE) as well as sensible (H) and latent (LE) heat fluxes, with ancillary climatological variables monitored to aid in data interpretation. The challenge is that at sites where the primary focus is on measuring carbon and water fluxes as is the case with AmeriFlux, the frequency of pyranometer calibration may be longer than is ideal because of funding constraints or a greater emphasis on maintaining more complicated instrumentation, such as eddy covariance systems. The AmeriFlux network deploys roving tower measurement systems for periodic QA/QC of turbulent fluxes and meteorological variables to help maintain network-wide data integrity, and have reported low average relative instrument errors of $-0.57 \pm 0.535\%$ (se) for $K\downarrow$ (Schmidt et al., 2012). However, with 100 active sites at the time of their publication and an average of 8.5 site visits per year between 2002 and 2012 (Schmidt et al., 2012), the time between inter-comparisons for a given location would be on the order of ~12 years.

Sites were selected such that there would be locations characterized by higher (<35°N, desert), mid-range (40–45°N) and lower (>50°N) levels of solar radiation exposure. Measurements of $K\downarrow$ were made using PSP and CM3 pyranometers. In the cases where the CM3 was used it was a component of a CNR1 four component net radiometer (Kipp and Zonen USA Inc., Bohemia, NY). The reported non-stabilities of the PSP and CM3 are ± 0.5 and $\pm 1\%\,y^{-1}$, respectively. The $K\downarrow$ data posted for one site (CA-Obs) was a PI-preference, which indicates that the time-series were a synthesis of their highest quality data. These data were examined in the context of identifying discontinuities associated with merging data from multiple sensors. Refer to the supplementary information for the $K\downarrow$ and PAR data included in this analysis (Fig. S2). Clear differences in the solar radiation environments of the three broad groupings were evident.

3. Results and discussion

3.1. Observed calibration drift

Ensemble average $K\downarrow$ data collected during the inter-comparison are provided in Fig. 2. Note that the data filtering did not eliminate daily maxima. Observed systematic differences between the sensors were most evident at around solar noon when $K\downarrow$ was near the daily maximum. The BW measurements were systematically higher than all the PSPs, while the two PSPs that had historically been deployed facing 'down' were similar, and always higher than the other PSPs that had been mounted facing 'upwards'. There was excellent agreement between the 'downward' facing PSPs, with a linear regression slope of 1.002 ± 0.0033 (se) ($p < 0.001$), and an insignificant intercept of $-1.9 \pm 1.8\,W\,m^{-2}$ ($p = 0.295$). Forcing through the origin resulted in a slight decrease in the slope estimate to 0.998 ± 0.0009 ($p < 0.001$). Because of the excellent agreement, the mean of the data from these two sensors was used in subsequent analyses involving the 'downward' facing PSPs.

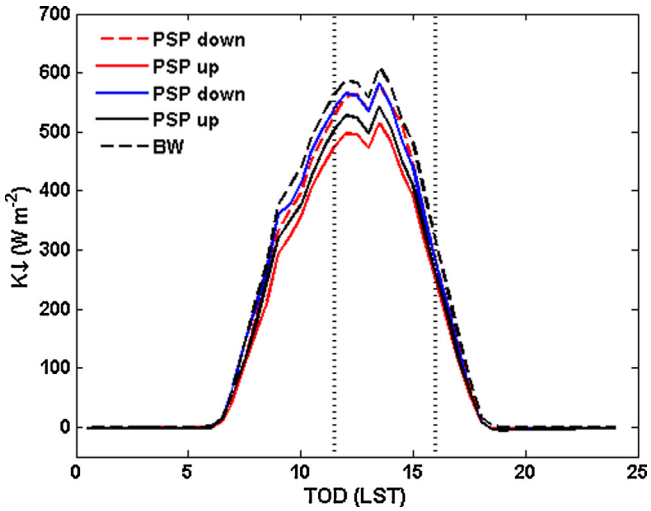

Fig. 2. Ensemble averaged incoming solar radiation ($K\downarrow$) measured during the sensor inter-comparison from Sep 20 through 30 (DOY 263–273) 2013. Data between the vertical dotted lines were retained for regression analyses.(For interpretation of the references to color in this figure legend, the reader is referred to the web version of this article).

Upon regressing the 'upward' facing G21 and I10 PSP signals against the mean signal from the 'downward' PSPs, differences in responsivities were found as evidenced by different slopes that diverged from unity ($slope_{G21} = 0.880 \pm 0.0011$; $slope_{I10} = 0.935 \pm 0.0024$) (Fig. 3a and b). This was expected, because a discoloration of the black paint on the sensing elements (to a noticeable green tint) on the 'upward' PSPs had been observed (e.g., Fig. 3c vs. d), with more severe fading noted for the G21 sensor. This discoloration represents a decreased absorptivity of the sensing element, which causes a systematic underestimation of $K\downarrow$. The green discoloration indicates an increased reflectivity in the green band of the solar spectrum, thus the downward calibration drift was accompanied by a change in spectral response. The G21 upward PSP should display larger bias due to the more severe discoloration, an assertion that was supported by the greater underestimation of $K\downarrow$ revealed by regression analyses (Fig. 3a). A subset of historical radiation data was analyzed to further examine this degradation in responsivity.

Data from the two 'upward' PSPs were compared to a co-located BW for years 2006–2010. In this case, BW data were used as the reference $K\downarrow$ measure. This may seem counterintuitive because BW

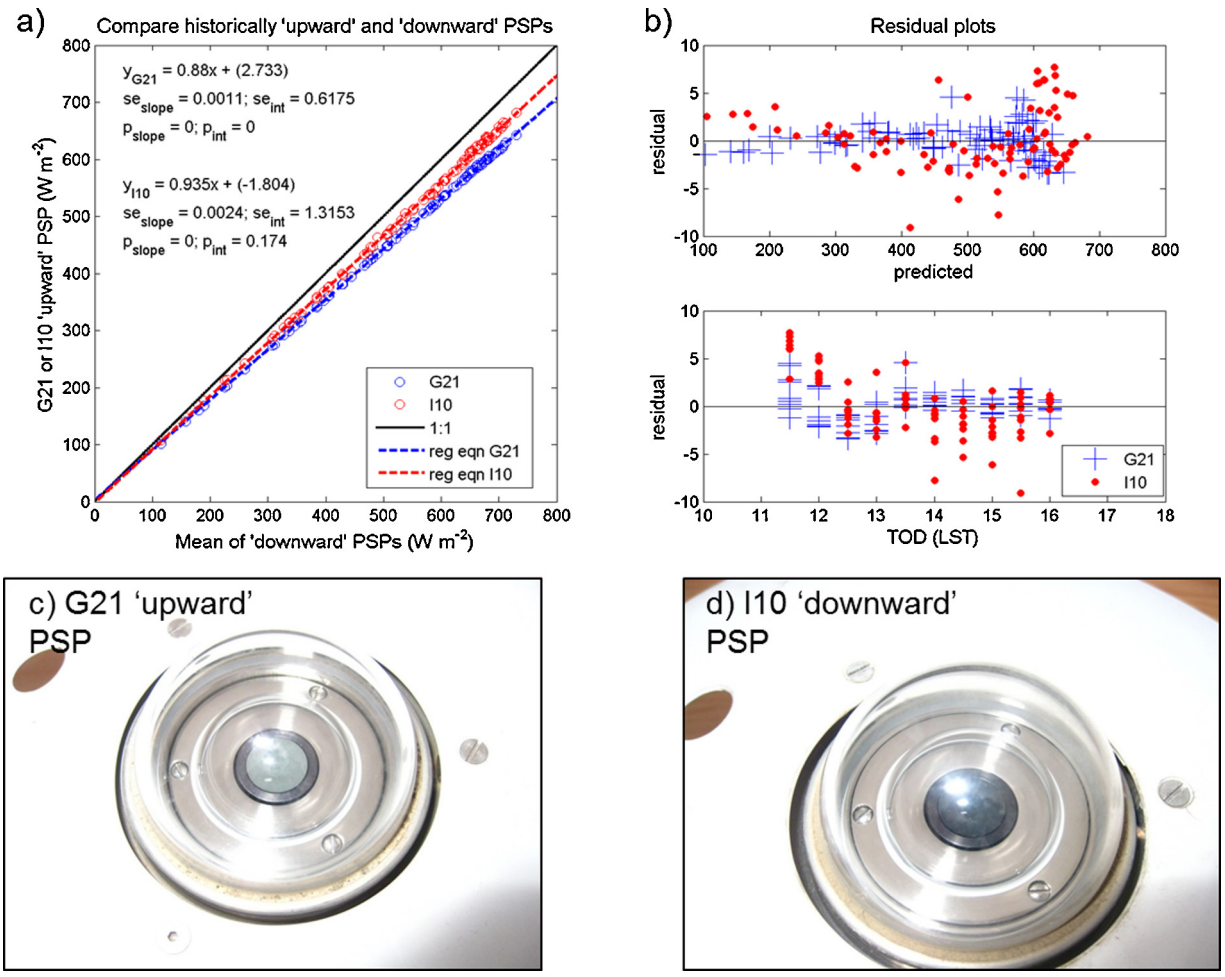

Fig. 3. Comparison of upward facing PSPs with downward facing PSPs. Panel (a) displays the results of the regression analyses, and panel (b) the residuals as a function of predicted values (upper) and time-of-day (lower). Panels (c) and (d) are photographs of discolored and normal PSP sensing elements. The greening discoloration causes the underestimation of radiation. (For interpretation of the references to color in this figure legend, the reader is referred to the web version of this article.)

pyranometers are classed lower than PSPs according to the WMO, because their directional responses deviate further from the ideal case than do PSPs. However, data from the 'upward' PSPs were suspect due to the noted discoloration (Fig. 3c). To minimize the effect of directional response errors in the historical analyses, more stringent filtering was performed whereby data were limited to solar zenith angles <65°. For each year, half-hourly average PSP responses were regressed against the BW responses. The slopes from these regressions were used as estimates of the PSP responsivity relative to the BW (which was stable) in each year. Relative responsivities deviating from a value of 1 indicate that the responsivity of the PSP is changing compared to the BW, with trends yielding estimates of the magnitude and direction of PSP drift.

The PSP responsivities decreased linearly from 2006 to 2010 (Fig. 4a). Although the absolute responsivities differed between PSPs, the temporal trend was similar. Indeed, the slopes of linear fits to each data series did not differ significantly according to a *t*-test ($p = 0.921$). The mean rate of responsivity decay was estimated as $-1.5 \pm 0.19\%\,y^{-1}$. This rate of decline was within the range noted in Riihimaki and Vignola (2008), which summarized several sources and reported decreases in PSP responsivities of up to $1.9\%\,y^{-1}$. They also pointed out that exposure to radiation was the critical factor in determining the rate of decay, which supports the findings in this inter-comparison where there was no visible color change for the 'downward' PSPs (Fig. 3c vs. d). To further explore the responsivity decay, a relationship with radiation exposure was established.

Upward facing PSP responsivities as a function of cumulative integrated $K\downarrow$ (measured by a BW) are provided in Fig. 4b. The general trend was similar to the time-dependent relationship, because for upward facing pyranometers, time is an excellent proxy for radiation exposure. As was the case with time as the explanatory variable, there was no difference in the responsivity decay rate according to a *t*-test ($p = 0.940$). The mean responsivity degradation rate as a function of radiation exposure was $-0.38 \pm 0.054\%$ $(GJ\,m^{-2})^{-1}$. From 2006 to 2013, the exposures of the G21 and I10 'downward' PSPs were ~6.3 and ~7.2 $GJ\,m^{-2}$, respectively. Assuming degradation caused by radiation exposure is an integrated effect that is independent of intensity or spectral characteristics, the resultant decreases in responsivity for the G21 and I10 downward PSPs were predicted to be 2.4% and 2.7%, respectively. The importance of radiation exposure in decreasing responsivity is underscored by the fact that the 'downward' PSPs did not suffer the same level of degradation as the 'upward' facing sensors (Fig. 3a), however, the fact that they were biased low compared to the BW sensor (Fig. 2) suggests that there was some downward calibration drift.

The cause of the stark differences in the absolute responsivities during 2006–2010 (Fig. 4) for the G21 and I10 'upward' PSPs is unclear because they were deployed at similar times. It is possible that the paint used on the sensing elements came from different batches and that the one used for the G21 'upward' PSP was less stable.

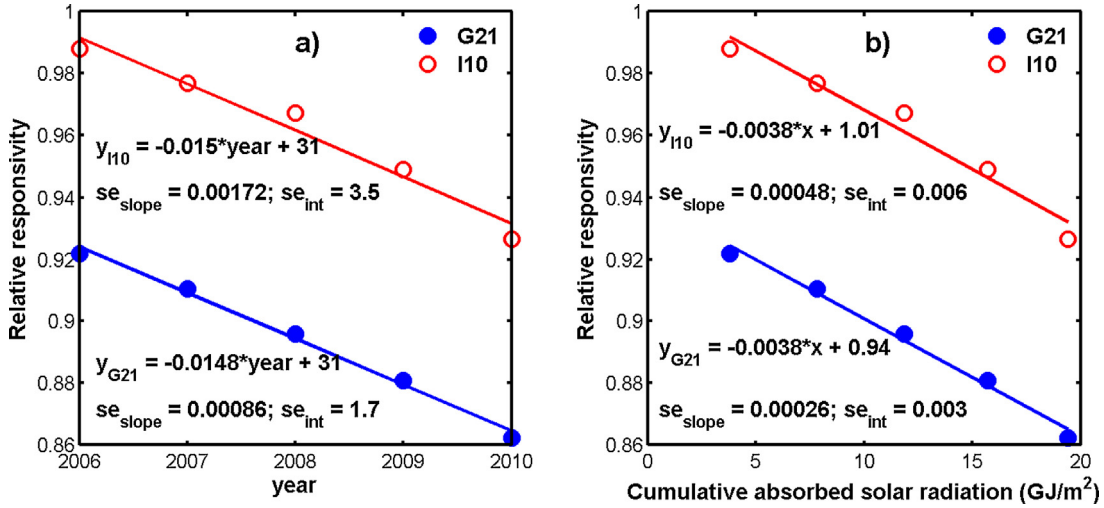

Fig. 4. Change in PSP (a) responsivities for a subset of years (2006–2010), and (b) the responsivities as a function of absorbed solar radiation (GJ/m^2). All regression parameters were significant ($p < 0.01$). Each symbol represents a relative responsivity that was calculated as the slope of a linear regression of the broadband incoming solar radiation fluxes measured by PSP's on measurements from a black and white pyranometer that was stable. Deviations from a value of 1 are reflective of a drifting PSP sensor. The slopes represent drift estimates for each PSP.

This analysis of responsivities assumed that the BW pyranometer was stable over time. In an effort to test the validity of this assumption, the annual mean ratios of PAR to $K\downarrow$ measured by the BW were examined to identify possible changes in BW responsivity. Therefore, if the PAR/$K\downarrow$ ratio exhibited a temporal trend it was expected to be due to a change in BW sensor characteristics. Linear fits of PAR vs. $K\downarrow$ fluxes were calculated for each year, and the slope taken as the estimate of the annual PAR/$K\downarrow$ ratio. The PAR/$K\downarrow$ ratio ranged from 0.48 to 0.51, and there was no temporal trend, as evidenced by an insignificant slope parameter estimate ($p = 0.498$) supporting the assertion that the BW was relatively stable from 2006 to 2010.

In summary, PSP responsivities clearly decreased as a function of radiation exposure. It appears that degradation may differ among individual PSPs based on the quality of the paint used on the sensing elements, and that 'good' quality paint may have an initial stable period. However, once responsivity decay began, the rates were similar and relatively constant as a function of radiation exposure at $0.38 \pm 0.054\%\,(\mathrm{GJ\,m^{-2}})^{-1}$. For a site like Rosemount MN with annual insolation of approximately $3.95\,\mathrm{GJ\,m^{-2}\,y^{-1}}$, this corresponds to a time-dependent decay of $1.5 \pm 0.19\%\,\mathrm{y^{-1}}$.

A critical point of note is that the declining responsivity was accompanied by a change in spectral response owing to the discoloration of the black paint on the sensing element. In this case, routine calibration procedures will correct the responsivity for the specific conditions during the procedure. Once re-deployed, the calibrated pyranometer will only be accurate when incident radiation has the same spectrum as the calibration radiation source, which may not be the case. For instance, the spectral distribution of K↑ varies with surface conditions, and differs from $K\downarrow$ (Michalsky and Hodges, 2013). The only remedy for the discoloration issue is re-conditioning (i.e., re-painting) the sensing element prior to calibration. Careful examination of the sensing elements of all-black pyranometers, and PSP's in particular, is therefore, recommended to guard against discoloring sensing elements. We found that outdoor, ambient light conditions made it difficult to discern the discoloration except for the most extreme case – it was, however, more noticeable indoors under fluorescent lights.

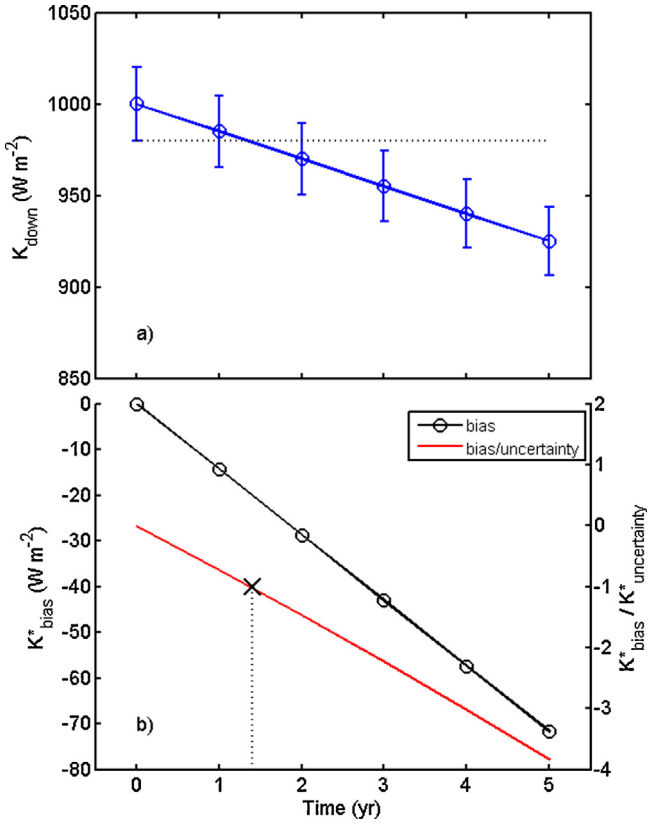

Fig. 5. Implications of pyranometer drift on (a) incoming (K_{down}) and net (K^*) solar radiation over time, assuming a true incoming solar radiation of 1000 W m^{-2}, and a surface albedo of 0.13. In (a) the error bars represent the measurement uncertainty (±2%) and the horizontal dotted line represents the lower limit of uncertainty in the initial year of deployment. In (b) the black line represents the bias in K^* and the red line represents the ratio of the bias to the measurement uncertainty ($K^*_{bias}/K^*_{uncertainty}$). The × and vertical dotted line indicate the time at which $K^*_{bias}/K^*_{uncertainty}$ equals 1 and thus, bias equals uncertainty. (For interpretation of the references to color in this figure legend, the reader is referred to the web version of this article).

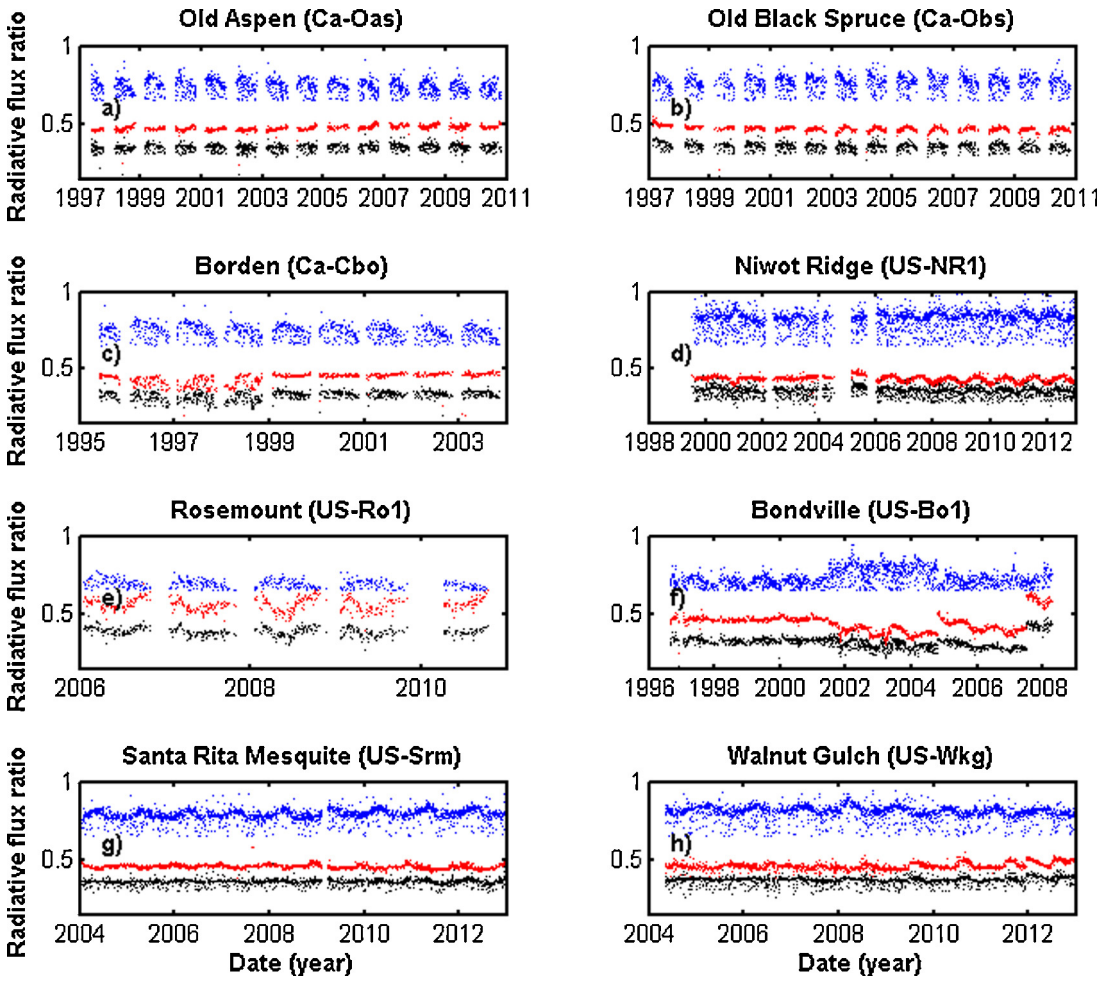

Fig. 6. Time-series of $K\downarrow/K_{EX}$ (blue), PAR/$K\downarrow$ (red), and PAR/K_{EX} (black) ratios for $K\downarrow/K_{EX} > 0.65$ (PAR = photosynthetically active radiation, $K\downarrow$ = incoming solar radiation at the surface, K_{EX} = extraterrestrial solar radiation at the top of the atmosphere). Each observation is the ratio of the daily maxima of the respective radiation variables. Observations are only shown when the solar zenith angle was >65°. (For interpretation of the references to color in this figure legend, the reader is referred to the web version of this article).

3.2. Implications of drift on measurements

For context, we illustrate the magnitude of the biases imparted by radiation exposure induced drift, by demonstrating the change over time of measured hourly average $K\downarrow$ and net surface solar radiation (K^*) when the pyranometers are affected by drift. We assumed clear-sky conditions and an hourly average $K\downarrow$ of 1000 W m^{-2}, a surface albedo of 0.13, the total uncertainty in hourly $K\downarrow$ was ±2% (Eppley PSP stated uncertainty) and did not change; and that the drifts were −1.5% y^{-1} and −0.5% y^{-1} for the upward and downward facing pyranometers, respectively. For both $K\downarrow$ and K^*, the bias equals the measurement uncertainty after ~1.5 years, while after three years the bias is large enough to be disentangled from the measurement uncertainty (Fig. 5). After 5 years, the bias was estimated to be −70 W m^{-2} for K^*, which could have large ramifications when assessing eddy covariance energy budget closure, conducting Penman Monteith or Bowen ratio measurements, or making radiative forcing calculations.

3.3. Drift detection in historical time-series

To extend our analysis, we examined data from several AmeriFlux sites for drift errors to determine whether the issue is of widespread concern. For context, the radiation environments of the sites are summarized in Fig. 6 showing only data where $K\downarrow/K_{EX}$ exceeded 0.65. While it was in general not possible to discern drift by eye, it was possible to identify potential issues in several of the time-series. The first 4 years of data at the CA-Cbo data exhibited larger seasonal variation than the last 4 years, particularly for ratios that contained PAR (Fig. 6c). The US-NR1 data also exhibited different seasonal patterns in the first half of the data set compared to the latter half (Fig. 6d). Finally, several large step changes were evident in the data from US-Bo1.

Example algorithm output with an accompanying interpretation can be found in the supplementary information (Fig. S3). Probable drift was diagnosed at five sites (5 pyranometers and one PAR sensor; Table 4), although the trends were not always what was expected. At Rosemount, we observed decaying PSP responsivities consistent with the notion that it was caused by solar radiation exposure for the two 'upward facing' PSPs discussed in section 3.1 (G21 and I10 upward), with significant PAR/$K\downarrow$ increases and $K\downarrow/K_{EX}$ decreases of similar magnitudes ($p > 0.05$) and no trend in the PAR/K_{EX} data. This is an important finding because we know that these PSPs were drifting. The findings were similar at CA-Oas, another site employing a PSP. At two sites (US-Srm US-Wkg), the analyses indicated positive pyranometer drift. In these cases, PAR/$K\downarrow$ decreased while $K\downarrow/K_{EX}$ increased over time. This suggests that the issue of physical changes in the sensing

Table 4
Slopes (±se) of the linear fits obtained when the drift detection algorithm terminated and decisions relative to drift detection. Values of 0 are reported when the slope parameter estimate was insignificant ($p > 0.05$). Within rows, the magnitudes of non-zero slope estimates followed by the same letter are not different ($p < 0.05$) according to a *t*-test.

Site	Years[a]	Slope × 10^{-5} (1/d)			Change points[b]	Drift detection summary[c]
		PAR/$K\downarrow$	$K\downarrow/K_{EX}$	PAR/K_{EX}		
Data from Rosemount, MN[d]						
PSP up G21	2006–2010	3.2 (0.59) a	−3.2 (0.44) a	0	N	$K\downarrow$ drift down
PSP up I10	2006–2009	1.5 (0.51) a	−3.3 (0.52) a	0	N	$K\downarrow$ drift down
Data from other AmeriFlux sites						
CA-Oas	2000–2004	1.0 (0.17) a	−1.8 (0.42) a	0	N	$K\downarrow$ drift down
CA-Obs	1997–2001	−1.3 (0.15) a	0	−1.3 (0.22) a	N	PAR drift down
CA-Cbo	1995–2003	0.7 (0.07) a	−1.0 (0.19) a	0	Y	Consider change point model
US-NR1	2001–2007	−0.2 (0.09) a	0.4 (0.19) a	0	Y	Consider change point model
US-Bo1	1998–2007	−2.7 (0.22)	1.2 (0.30)	−1.4 (0.11)	Y	Consider change point models
US-Srm	2004–2010	−0.2 (0.08) a	0.4 (0.18) a	0	N	$K\downarrow$ drift up
US-Wkg	2005–2008	−0.9 (0.24) b	2.4 (0.46) a	0	N	$K\downarrow$ drift up

[a] The years for which summarized results were obtained.
[b] Interpretation requires consideration of significant change points; Y = yes, N = no.
[c] Conclusions based on results from linear fits and the presence/absence of significant change points. The results for cases where it was necessary to consider change point models are presented in Fig. 7. $K\downarrow$ drift down = downward drifting pyranometer; $K\downarrow$ drift up = upward drifting pyranometer; PAR drift down = downward drifting PAR sensor.
[d] In the site column, Rosemount pyranometer designation corresponds to the previously established nomenclature in this present work.

element causing a decrease in the responsivity of the sensing element was not an issue with these pyranometers, but that there were errors caused by some other factor contaminating the $K\downarrow$ data. These two sites employed CM3 pyranometers as component sensors on CNR1 net radiometers. It may be that drift in the shunt resistors, which trim the output voltages of the component sensors to a common sensitivity, were causing the upward drift in the CM3 signals. Another interesting finding was that at CA-Obs, where the $K\downarrow$ was a synthesis of PI-preferred measurements, we detected drift in the PAR sensor. In this case, there was no significant trend in $K\downarrow/K_{EX}$, however, both PAR/$K\downarrow$ and PAR/K_{EX} displayed significant decreasing trends of similar magnitudes ($p > 0.05$).

Although there were significant linear trends at CA-Cbo and US-NR1 (Table 4), there were significant change points that must be considered in these cases (Fig. 7). At CA-Cbo there were change points found for each ratio in either 1997 or 1998. For each flux ratio, the intercepts were different before and after the change point, which suggests that there could have been a recalibration, re-leveling or sensor replacement. Further, the ratios that include PAR displayed high variability about a highly negative trend prior to the change points, which was not the case in segment 2. Based on these observations further investigation of PAR data prior to the change point seems warranted. After the change point both $K\downarrow/K_{EX}$ and PAR/K_{EX} decreased and $K\downarrow/K_{EX}$ increased over time obscuring drift detection after the change point. At US-NR1, our analysis did not conclusively find evidence of sensor drift (Fig. 7), however, significant change points were found for all radiative flux ratios at US-NR1, which may have been due to other artifacts such as sensor leveling or calibration. Similar to US-NR1, the analyses did not identify drift at US-Bo1 (data not shown). In the case of US-Bo1, there were changes in $K\downarrow$ and PAR data that could be identified by eye in either time series of the radiative flux ratios (Fig. 6f) or the raw fluxes (Fig. S2). This partitioned the data into several segments and interfered with drift detection. It is noteworthy that the algorithms were inconclusive at the three sites for which observations by eye of the raw data indicated possible issues.

This analysis was devised to minimize the effects of natural variations in atmospheric transmissivity on drift detection. As noted previously, water vapor absorbs in the infrared region and is of greatest concern because it only affects $K\downarrow$. To confirm that variations in water vapor did not contaminate these analyses, we examined surface vapor pressures (e_a) observed during the averaging periods that were selected by the algorithm. Although shortwave absorption is related to column-integrated water vapor, e_a is a useful indicator of atmospheric moisture status in the absence of co-located measurements of the former. The results of this analysis are summarized in Fig. S4. The relation between $K\downarrow/K_{EX}$ and e_a followed exponential decay, with site-specific coefficients due to differences in mean moisture status and elevation (Fig S4a). However, since we were preferentially selecting for the clearest-sky days with high transmissivity, the range of e_a within-years was generally similar (Fig. S4b). That is, variable moisture conditions affected within-year variations in the $K\downarrow/K_{EX}$ and PAR/$K\downarrow$ ratios, rather than the temporal trends. Indeed, linear regression analysis of the annual (i) median e_a and (ii) interquartile range of e_a on years yielded insignificant slopes at all sites ($p > 0.1$). To summarize, although water vapor affects atmospheric transmissivity, in the context of our drift detection routines the within-year effects are more important because the sampling strategy tends to draw from consistent ranges of moisture across years. The implication is that variable e_a is partially responsible for noise in the signal, making it more difficult to diagnose drift, as opposed to exerting controls on the trends in $K\downarrow/K_{EX}$ and PAR/$K\downarrow$ ratios over time.

One of the shortcomings of this approach is that several years of data are required before one can confidently ascribe trends in the ratios to measurement errors, however, this is not an issue when assessing historical data. In the cases where there was pyranometer drift, 3–6 years of data were required before a significant linear trend was observed. While this has the disadvantage that it does not immediately identify when a sensor begins drifting, it is implemented to prevent falsely identifying inter-annual variations in optical depth or other artifacts as drift. These approaches can be incorporated into QA/QC routines at active measurement sites as a relatively simple and effective way to track the performance of radiation sensors.

3.4. Other QA/QC considerations: exposure error

The drift detection algorithms were designed to restrict the analyses to periods with the highest $K\downarrow/K_{EX}$ to minimize the impact of natural variations in optical depth, which necessarily imparts substantial data reduction. This approach was designed to specifically eliminate as many confounding errors as possible. Examining intermediate output from analyses of daily correlation coefficients between (i) $K\downarrow$ and K_{EX} and (ii) PAR and K_{EX} data revealed time periods (e.g., one site-year at a location) where the PAR sensors

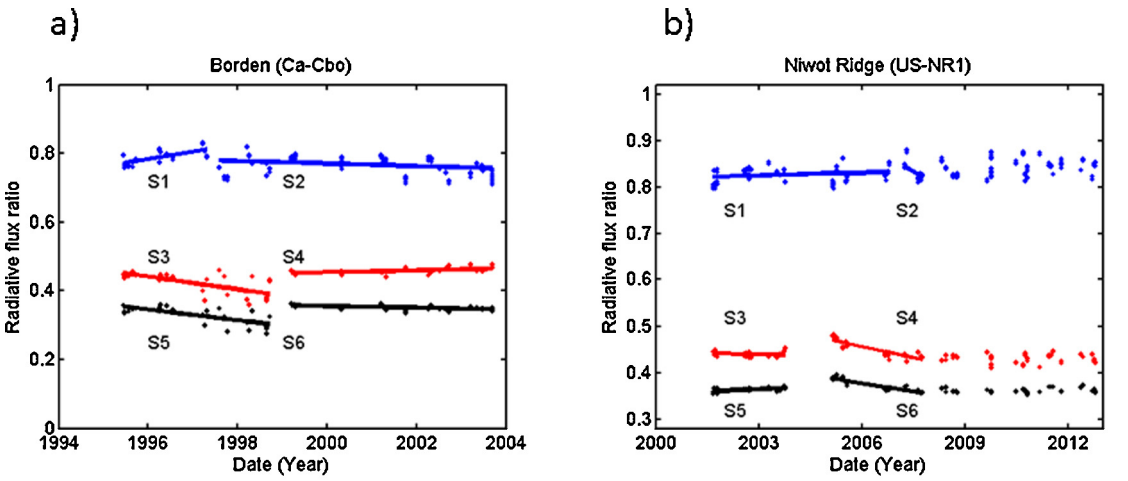

Ratio	Segment	Slope (se) × 10^{-5}
$K\downarrow/K_{EX}$	S1	5.9 (0.87)
	S2	-1.0 (0.31)
PAR/K↓	S3	-5.1 (0.65)
	S4	0.8 (0.15)
PAR/K_{EX}	S5	-4.2 (0.51)
	S6	-0.6 (0.11)

Ratio	Segment	Slope (se) × 10^{-5}
$K\downarrow/K_{EX}$	S1	0.6 (0.24)
	S2	-12.9 (2.33)
PAR/K↓	S3	0
	S4	-4.4 (0.33)
PAR/K_{EX}	S5	0.9 (0.19)
	S6	-3.2 (0.22)

Fig. 7. Summary of change point model results for (a) Borden (Ca-Cbo) and (b) Niwot–Ridge (US-NR1) sites fitted to $K\downarrow/K_{EX}$, (blue symbols and line), PAR/$K\downarrow$(red symbols and line) and PAR/K_{EX} (black symbols and line) ratios ($K\downarrow$ = incoming solar radiation, PAR = incoming photosynthetically active radiation, and K_{EX} = incoming extraterrestrial radiation at the top of the atmosphere), with the standard errors for each. The slopes with standard errors for each segment are tabulated below the respective graph panels, where values of 0 are shown when the slope was not significant according to a t-test ($p > 0.05$). Note that the entire time-series of raw data are shown, while the predicted values (lines) are extended only to the time at which the algorithms terminated. (For interpretation of the references to color in this figure legend, the reader is referred to the web version of this article).

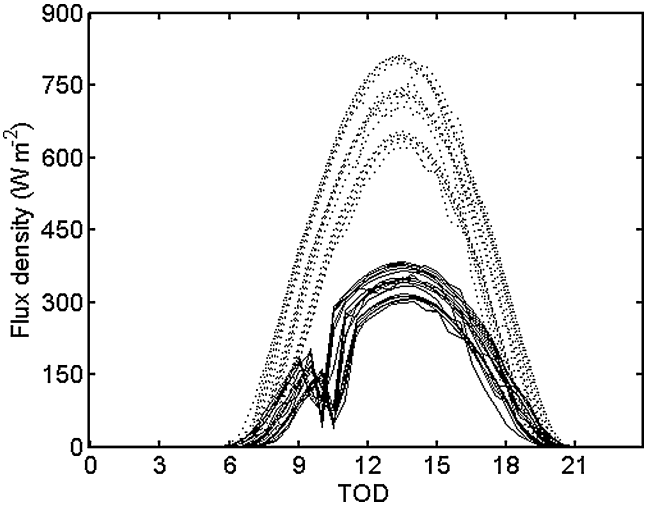

Fig. 8. Example diurnal variations of incoming solar radiation ($K\downarrow$, dotted black lines) and photosynthetically active radiation (PAR, solid black lines) for the same days, where the PAR sensor displayed responses that typify exposure errors associated with shading.

had been deployed in a position that was partially shaded in the mornings, which resulted in underestimations of half-hourly measurements of ~100 W m^{-2} on clear sky days (Fig. 8). Although this artifact did not affect our drift detection analyses, it further highlighted the need for careful data screening.

Our analyses identified exposure errors, probable drift and other artifacts in historical AmeriFlux radiation data from several sites. Considering that recent reductions in globally averaged $K\downarrow$ have been estimated at 2.7% per decade (Stanhill and Cohen, 2001), the drift reported here is sufficient to contaminate analyses of long-term temporal trends. Although considering multiple years of data at each site is laborious, we have shown the value in evaluating long-term data records with post-hoc screening to identify bias. Further, the frequent incidence of drift suggests the need to increase network-wide calibration frequency. While this is in part fulfilled by the AmeriFlux mobile QA/QC systems (Schmidt et al., 2012), the number of sites that can be visited each year is limited. Some form of centralized calibration service where site PIs are able to ship sensors is one way to promote increased calibration frequency.

4. Conclusions

We demonstrated that calibration drift for Eppley PSP pyranometers was caused by a radiation-induced discoloration of the sensing element that altered the spectral response. An initial stable

period that varied among sensors was observed, but once responsivities began to decay, they declined at similar rates that were linearly related to radiation exposure, which for a mid-latitude site represented drift of $-1.5\%\,y^{-1}$. At this rate, the drift bias exceeds the total measurement uncertainty after ~3 years. After 5 years, without calibration, K^* is underestimated by $\sim 70\,W\,m^{-2}$, which is enough to have large implications on applications requiring accurate measurements of available energy such as eddy covariance energy balance closure, or Penman-Monteith or Bowen ratio methods. The altered spectral response is also critical in the context of maintaining high quality measurements because calibration will not account for the change in spectral response unless the sensing element is first re-painted.

We have proposed the use of $K\downarrow/K_{EX}$, PAR/$K\downarrow$ and PAR/K_{EX} ratios to diagnose calibration drift and other errors in $K\downarrow$ time-series. In the absence of issues that cause noticeable step changes in the data, the method was able to diagnose possible drift. This can be used as additional QA/QC on $K\downarrow$ data at active measurement sites to determine when calibration is needed, or for post-hoc screening when synthesizing data from many sites. We diagnosed drift in $K\downarrow$ data collected at multiple AmeriFlux sites. Downward drift that was consistent with fading of the sensing element was observed at several sites deploying PSPs. We also found upward drift at two sites employing the CM3 as a component sensor of a CNR1 net radiometer, which was possibly caused by drift in the shunt resistor. The utility of collectively examining these ratios to easily flag periods of data that may be suspect was highlighted. We were also able to identify sensors that experienced shading exposure error, which biased measurements by up to $-100\,W\,m^{-2}$ on clear sky days. Incorporating these approaches into QA/QC programs could help to improve data integrity at active sites, and when assimilating data from many sites for reanalysis. Although this method is not without drawbacks because it relies on co-located measurements, one of which must be stable, it was developed in an attempt to provide a practical solution to a challenging problem in order to maximize the use of existing datasets. Finally, this analysis highlights that greater availability of economical access to network-managed calibration services would be of value from the perspective of increasing calibration frequency.

Acknowledgements

We would like to acknowledge the technical support provided by Bill Breiter, as well as the site PI's from other AmeriFlux sites: T.A. Black, P. Blanken, T. Meyers, R. Scott and R. Staebler. Support for this research was provided by the United States Department of Agriculture, Grant number: USDA-NIFA 2013-67019-21364 and the Minnesota Corn Research & Promotion Council (4101-14SP). We would also like to acknowledge the AmeriFlux core site funding provided by the United States Department of Energy's Office of Science.

Appendix A. Supplementary data

Supplementary data associated with this article can be found, in the online version, at http://dx.doi.org/10.1016/j.agrformet.2015.02.015.

References

Amiro, B., Barr, A., Black, T., Iwashita, H., Kljun, N., Mccaughey, J., Morgenstern, K., Murayama, S., Nesic, Z., Orchansky, A., 2006. Carbon, energy and water fluxes at mature and disturbed forest sites Saskatchewan. Can. Agric. For. Meteorol. 136, 237–251.

Arking, A., 1996. Absorption of solar energy in the atmosphere: discrepancy between model and observations. Science 273, 779–782.

Arora, V.K., Montenegro, A., 2011. Small temperature benefits provided by realistic afforestation efforts. Nat. Geosci. 4, 514–518.

Augustine, J.A., Hodges, G.B., Cornwall, C.R., Michalsky, J.J., Medina, C.I., 2005. An update on SURFRAD – the GCOS surface radiation budget network for the continental United States. J. Atmos. Oceanic Technol. 22, 1460–1472.

Baker, J.M., Griffis, T.J., 2005. Examining strategies to improve the carbon balance of corn/soybean agriculture using eddy covariance and mass balance techniques. Agric. For. Meteorol. 128, 163–177.

Baldocchi, D., Falge, E., Gu, L., Olson, R., Hollinger, D., Running, S., Anthoni, P., Bernhofer, C., Davis, K., Evans, R., Fuentes, J., Goldstein, A., Katul, G., Law, B., Lee, X., Malhi, Y., Meyers, T., Munger, W., Oechel, W., Paw, K.T.U., Pilegaard, K., Schmid, H.P., Valentini, R., 2001. FLUXNET: a new tool to study the temporal and spatial variability of ecosystem-scale carbon dioxide, water vapor, and energy flux densities. Bull. Am. Meteorol. Soc. 82, 2415–2434.

Bergeron, O., Margolis, H.A., Black, T.A., Coursolle, C., Dunn, A.L., Barr, A.G., Wofsy, S.C., 2007. Comparison of carbon dioxide fluxes over three boreal black spruce forests in Canada. Global Change Biol. 13, 89–107.

Betts, R.A., 2000. Offset of the potential carbon sink from boreal forestation by decreases in surface albedo. Nature 408, 187–190.

Bush, B.C., Valero, F.P.J., Simpson, A.S., 2000. Characterization of thermal effects in pyranometers: a data correction algorithm for improved measurement of surface insolation. J. Atmos. Oceanic Technol. 17, 165–175.

Campbell, G.A., Norman, J.M., 1998. An Introduction to Environmental Biophysics, 2nd ed. Springer Science + Business Media Inc., New York, NY.

Dutton, E.G., Michalsky, J.J., Stoffel, T.L., Forgan, B.W., Hickey, J., Nelson, D.W., Alberta, T.L., Reda, I., 2001. Measurement of broadband diffuse solar irradiance using current commercial instrumentation with a correction for thermal offset errors. J. Atmos. Oceanic Technol. 18, 297–314.

Georgescu, M., Lobell, D.B., Field, C.B., 2011. Direct climate effects of perennial bioenergy crops in the United States. Proc. Natl. Acad. Sci. U. S. A. 108, 4307–4312.

Haeffelin, M., Kato, S., Smith, A.M., Rutledge, C.K., Charlock, T.P., Mahan, J.R., 2001. Determination of the thermal offset of the Eppley precision spectral pyranometer. Appl. Opt. 40, 472–484.

Ji, Q., 2007. A method to correct the thermal dome effect of pyranometers in selected historical solar irradiance measurements. J. Atmos. Oceanic Technol. 24, 529–536.

Ji, Q., Tsay, S.-C., 2010. A novel nonintrusive method to resolve the thermal dome effect of pyranometers: instrumentation and observational basis. J. Geophys. Res. 115, D00K21.

Ji, Q., Tsay, S.-C., Lau, K.M., Hansell, R.A., Butler, J.J., Cooper, J.W., 2011. A novel nonintrusive method to resolve the thermal dome effect of pyranometers: radiometric calibration and implications. J. Geophys. Res. 116, D24105.

Leuning, R., van Gorsel, E., Massman, W.J., Isaac, P.R., 2012. Reflections on the surface energy imbalance problem. Agric. For. Meteorol. 156, 65–74.

Meyers, T., Hollinger, S.E., 2004. An assessment of storage terms in the surface energy balance of maize and soybean. Agric. For. Meteorol. 125, 105–115.

Michalsky, J.J., Hodges, G.B., 2013. Field measured spectral albedo-four years of data from the Western U.S prairie. J. Geophys. Res. Atmos. 118, 813–825.

Myers, D.R., Stoffel, T.L., Reda, I., Wilcox, S.M., Andreas, A.M., 2002. Recent progress in reducing the uncertainty in and improving pyranometer calibrations. J. Sol. Energy Eng. 124, 44–50.

Myhre, G., Shindell, D., Breon, F.-M., Collins, W., Fuglestvedt, J.S., Huang, J., Koch, D., Lamarque, J.-F., Lee D., Mendoza, B., Nakajima, T., Robock, A., Stephens, G., Takemura, T., Zhang, H., 2013. The Physical Science Basis Final Draft Underlying Scientific-Technical Assessment A report accepted by Working Group I of the IPCC but not approved in detail, in: Working Group I Contribution to the IPCC Fifth Assessment Report Climate Change.

Ohmura, A., Gilgen, H., Hegner, H., Müller, G., Wild, M., Dutton, E.G., Forgan, B., Fröhlich, C., Philipona, R., Heimo, A., König-Langlo, G., McArthur, B., Pinker, R., Whitlock, C.H., Dehne, K., 1998. Baseline surface radiation network (BSRN/WCRP): new precision radiometry for climate research. Bull. Am. Meteorol. Soc. 79, 2115–2136.

Philipona, R., 2002. Underestimation of solar global and diffuse radiation measured at Earth's surface. J. Geophys. Res. 107, 4654.

Potts, D.L., Scott, R.L., Cable, J.M., Huxman, T.E., Williams, D.G., 2008. Sensitivity of mesquite shrubland CO_2 exchange to precipitation in contrasting landscape settings. Ecology 89, 2900–2910.

Ramanathan, V., Feng, Y., 2009. Air pollution, greenhouse gases and climate change: global and regional perspectives. Atmos. Environ. 43, 37–50.

Ramanathan, V., Vogelmann, A.M., 1997. Greenhouse effect, atmospheric solar absorption and the Earth's radiation budget: from the Arrhenius–Langley Era to the 1990. R. Swed. Acad. Sci. 26, 38–46.

Riihimaki, L., Vignola, F., 2008. Establishing a consitent calibration record for Eppley PSPs, in: Proc. of the 37th American Solar Energy Society Conference. San Diego.

Schmidt, A., Hanson, C., Chan, W.S., Law, B.E., 2012. Empirical assessment of uncertainties of meteorological parameters and turbulent fluxes in the AmeriFlux network. J. Geophys. Res. 117, G04014.

Scott, R.L., 2010. Using watershed water balance to evaluate the accuracy of eddy covariance evaporation measurements for three semiarid ecosystems. Agric. For. Meteorol. 150, 219–225.

Stanhill, G., Cohen, S., 2001. Global dimming: a review of the evidence for a widespread and significant reduction in global radiation with discussion of its

probable causes and possible agricultural consequences. Agric. For. Meteorol. 107, 255–278.
Wang, K.C., Dickinson, R.E., Wild, M., Liang, S., 2012. Atmospheric impacts on climatic variability of surface incident solar radiation. Atmos. Chem. Phys. 12, 9581–9592.
Wang, X.L., 2003. Comments on detection of undocumented changepoints: a revision of the two-phase regression model. J. Clim. 16, 3383–3385.
Wild, M., Gilgen, H., Roesch, A., Ohmura, A., Long, C.N., Dutton, E.G., Forgan, B., Kallis, A., Russak, V., Tsvetkov, A., 2005. From dimming to brightening: decadal changes in solar radiation at Earth's surface. Science 308, 847–850.